# A New Elastic-wave-based NDT System for Imaging Defects inside Concrete Structures

Jian-Hua Tong and Shu-Tao Liao

***Abstract*— In this paper, a new elastic-wave-based NDT system was proposed and then applied to reveal the defects inside the concrete specimens by imaging method. In this NDT system, it integrates the point-source/point-receiver scheme with the synthetic aperture focusing technique (SAFT) to achieve the effect like scanning with a phase array system; hence it is equipped with large functioning depth because of the high-energy feature that transient elastic wave method possessed over traditional ultrasonic method. This system is mainly composed of an impact source generator, a vertical displacement transducer, a signal capturing unit and operation software. To evaluate the feasibility of this system on NDT of concrete structures, some concrete slabs with artificial voids inside were built for experiment. 2D plane stress FEM numerical simulations were performed for further comparison. Experimental result shows good agreement with the numerical result not only on the B-scan diagram but also on the processed scanning image. The elastic-wave-based scanning system proposed in this paper exhibits high potential in inspecting the defects of in-situ concrete structures by imaging for civil engineering applications.**

***Index Terms*—concrete, elastic wave, image, NDT.**

## I. Introduction

Among the present civil NDT technologies, the elastic-wave-based application always plays a very important role. The point-source/point-receiver scheme is especially suitable for the inspection of on-site civil infrastructures [1-6]. It overcomes the limitation of transmission distance caused by the nature of the traditional ultrasonic probing, which is featured by low output power. However, when these methods are applied to detect defects inside the real concrete structures, especially with complex boundary conditions or multiple inclusions, successful results are usually hard to obtain with analyzing a single batch of response signals. For metallic materials the synthetic aperture focusing technique (SAFT) is often used as a signal processing strategy in ultrasonic testing as a NDT method, good results of high S/N ratio can be obtained as those obtained with the phase array system [7,8]. In 2007, Tong et al. proposed a new elastic-wave-based imaging method, combining the point-source/point-receiver scheme and SAFT method, to reveal defects inside concrete structure by image [9]. It could be a practical and effective NDT method to detect defects inside civil infrastructures. To make this new NDT method more practical for in-situ application, it is indispensable to develop a new NDT system basing on above mentioned method. In this paper, the composition of this system was proposed. Some concrete slabs with artificial voids inside were built for evaluating the feasibility of this system on NDT of real concrete structures. The experimental results will demonstrate the potential of this system to be a helpful NDT tool for in-situ structure's defect diagnosis.

Manuscript received March 11, 2009. This work was supported by the National Science Council of ROC under Grants NSC 94-2211-E-241-017 and NSC 93-2211-E216-006.

Jian-Hua Tong is with the Department of Computer Science and Information Engineering, Hungkuang University, Taichung 433, Taiwan, ROC. (phone: 886-926269737; fax: 886-4-26324084; e-mail: jhtong@sunrise.hk.edu.tw).

Shu-Tao Liao is with the Department of Civil Engineering, Chung Hua University, Hsinchu 300, Taiwan, ROC.(e-mail: shutao@chu.edu.tw).

## II. Principle of Imaging

Shown in Fig.1 is a specimen to be tested. A series of impact-and-receive operations is performed on the free surface of the specimen. Let $S_i$ and $R_i$ represent the locations of a set of the source and receiver for the *i*-th measurement. Furthermore let $T_i(t)$ be the magnitude of the response signal recorded at $R_i$ for this measurement. The domain of the specimen is then divided into mesh grids. An image intensity $I(m,n)$ can be assigned to each grid based on the following calculation:

$$I(m,n)=\frac{1}{N}\sum_{i=1}^{N}T_i(t_i),\quad t_i=\frac{\left|\overrightarrow{S_iG(m,n)}\right|+\left|\overrightarrow{G(m,n)R_i}\right|}{C_P} \qquad (1)$$

where $G(m, n)$ is the t *m-th* row and *n-th* column grid in the domain, $N$ is the total number of the measurements, and $C_P$ is the

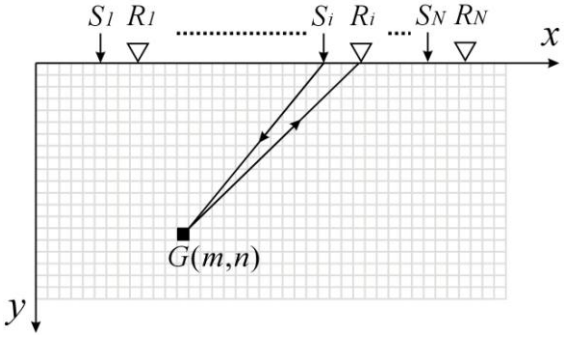


Fig.1 Schematic showing the implementation of impact-and-receive operations and meshing of specimen for image processing with SAFT.

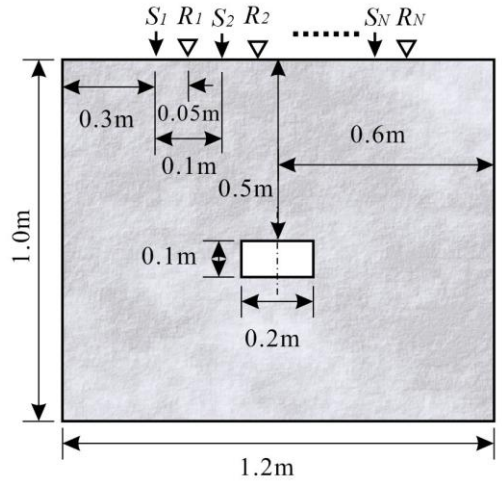


Fig.2 Dimensions of concrete specimen with rectangular void for the study of numerical simulation.

propagating velocity of the longitudinal wave.

According to the elastic wave theory, the wave will be reflected at the interface of two different media. The reflection could be found on the time domain signal if it could be sensed by the transducer. In general case, however, there are so many reflected signals from the boundaries and defects that determining the location of a defect from the complex trace is very hard. Besides, the dimension of defect is not easy to judge from only one time domain signal. In SAFT-imaging process, it extracts the information not just from one signal but from all the received signals to form the image. The image intensity I corresponding to each grid is determined by summing the amplitudes of all the measurements at the time ti and then taking the average value. The corresponding time of such point is the traveling time the wave propagating from source to grid point and then back to the receiver. With this process, the intensity will be summed up evidently when an interface exists right at the grid point and it will appear as a bright point. In contrast, it will be canceled out and appear as a dark point in the image. With this image processing scheme, the defects and interfaces embedded in the matrix material can be exposed. The resultant image will be similar to that scanned with a phased array system.

Consider a concrete block as a specimen. The cross section of the block is rectangular, and the dimension is 1.2m × 1m, as shown in Fig.2. Inside the block there exists a void with a rectangular section of 0.2m × 0.1m. Shown in Fig.3 is a typical B-scan diagram of displacement signals which is obtained by FDM simulation. These 13 traces are placed in upward order along the vertical axis. The fluctuations marked with "R" are associated with the arrival of Rayleigh waves. Those marked with "B" and "D" are associated with the reflections of longitudinal wave from bottom boundary and from defect respectively. Those marked with "RR" are associated with the reflections of Rayleigh wave from side boundaries. Using the algorithm and image processing technique described above to manipulate these 13 traces, a scan-like image can be obtained as shown in Fig.4. In this figure, a bright strip in the center, as enclosed by a dashed rectangle, indicates that there exists a

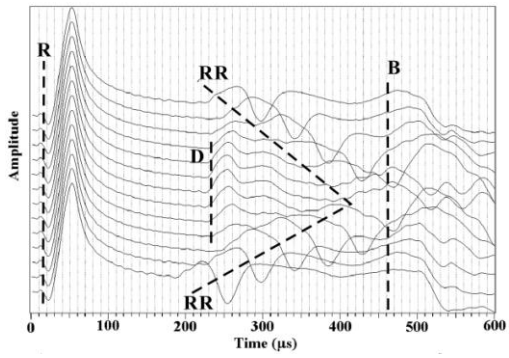


Fig.3 B-scan diagram of concrete specimen with single rectangular void in numerical simulation.

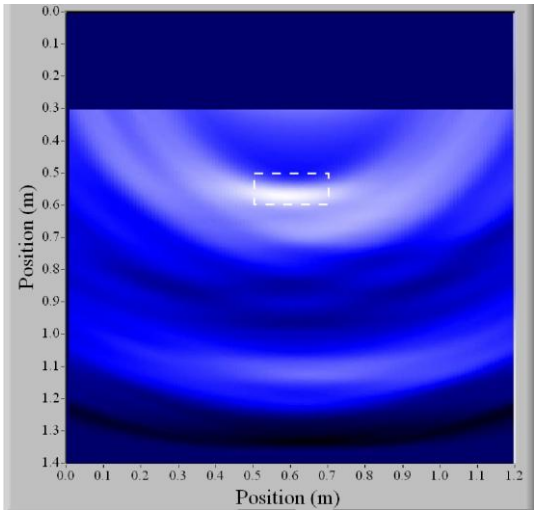


Fig.4 SAFT image generated from displacement responses of concrete specimen with single rectangular void in numerical simulation.

defect. From the figure, not only the location but also the width of the defect can be observed. A long bright strip associated with the bottom of the specimen can also be seen in the lower part of image. There is one thing need to note a horizontal strip with a thickness of 0.3m below the free surface is erased to a dark area so that it can enhance the contrast of the image by reducing the dynamic range which may be increased by Rayleigh wave.

## III. Composition of the New NDT System

It is very important that when applying a new NDT technology to in-situ application, a useful instrument is indispensable. An elastic-wave-based scanning system for SAFT-imaging on in-situ structures was proposed in this paper. It is mainly composed of an impact source generator, a vertical displacement transducer, a signal capturing unit and an operation software, as shown in Fig.5. The transient elastic wave is generated by a point impact on the surface of the specimen, and then propagates inside the material. The transducer then receives the surface response and converts it into an electrical signal. The signal capturing unit amplifies the small signal and converts the analog signal into digital data for

Table 1. Wavelength of elastic wave generated by different-sized steel ball impact.

| | Experimental result | | Hertz theory | | | λ |
|---|---|---|---|---|---|---|
| D(mm) | $f_c$(kHz) | λ(mm) | Tc(μs) | $f_c$(kHz) | λ(mm) | error |
| 2 | 44.8 | 50 | 9.87 | 47.5 | 47 | -5.7% |
| 3 | 34.2 | 66 | 14.81 | 33.1 | 68 | 3.3% |
| 4 | 24.0 | 94 | 19.75 | 26.4 | 85 | -9.1% |
| 5 | 15.6 | 144 | 24.68 | 19.0 | 119 | -17.9% |
| 6 | 13.4 | 168 | 29.62 | 15.9 | 142 | -15.7% |
| 7 | 11.2 | 201 | 34.56 | 13.6 | 166 | -17.6% |
| 8 | 10.4 | 217 | 39.49 | 11.9 | 189 | -12.6% |

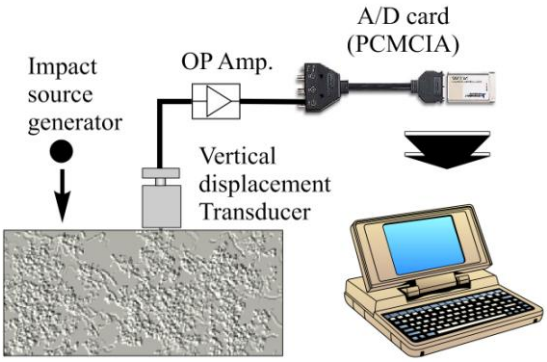


Fig.5 Composition of the elastic-wave-based scanning system.

further process. The operation software controls all the measurement procedure and finally develops the image according to the method described above.

### A. *Impact Source Generator*

The source generator is made of a steel bar with a steel ball weld on the end. To generate elastic wave, the steel bar is bent and then released to hit the surface of specimen. The force-time function of impact is almost in the form of half cycle $sin^{3/2}t$ function. Derived from Hertz contact theory, the contact time $T_C$ could be obtained by following calculation:

$$T_C = 8.034\left[\frac{\rho_1(\delta_1+\delta_2)}{v_0^{1/2}}\right]^{2/5} R \qquad (2)$$

While $$\delta_1 = \frac{1-\nu_1^2}{\pi E_1} \qquad \delta_2 = \frac{1-\nu_2^2}{\pi E_2} \qquad (3)$$

Where $\nu$ is Poisson's ratio, $E$ is Young's modulus. The subscript 1 and 2 represent the character of steel ball and that of half-space material respectively. $R$ denotes the radius of steel ball. From Eq. 2, it is clear that the larger the steel ball, the longer the contact time and thus the larger the wavelength of elastic wave. According to Eq. 2, Table 1 shows the theoretical value and experimental value of wavelength while elastic wave is generated by steel ball impact in different size. The result shows high capability of Eq. 2 to be the guidance for selection of steel ball when making the trade-off between resolution and detectable depth for inspection.

### B. *Vertical Displacement Transducer*

The vertical displacement transducer converts the mechanical displacement signal into electrical signal. As shown in Fig.6, it is mainly composed of a vertically polarized PZT ceramic cone, backing material and the holding fixture. The PZT ceramic cone will produce an electric potential difference, i.e. voltage signal, between two electrodes when suffered longitudinal deformation. The upper electrode is electrically connected to the backing brass block and then to the BNC connector as the signal source. The lower electrode is connected to the copper film, the metal holding fixture and finally the BNC connector as the electrical ground. For better contact condition between PZT tip and uneven concrete surface, the lower part of backing brass is shaped inclined. The backing container, holding the backing brass, can slide freely along the longitudinal direction of the holding fixture so that PZT tip can reach the measurement point precisely.

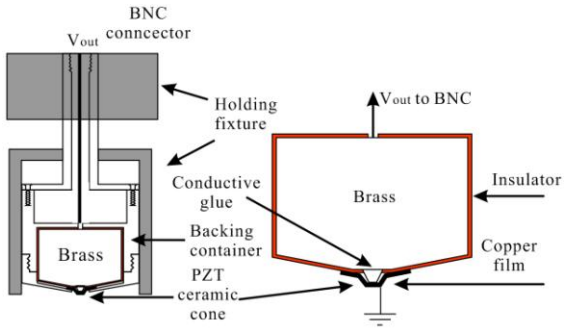


Fig.6 Scheme of the vertical displacement transducer.

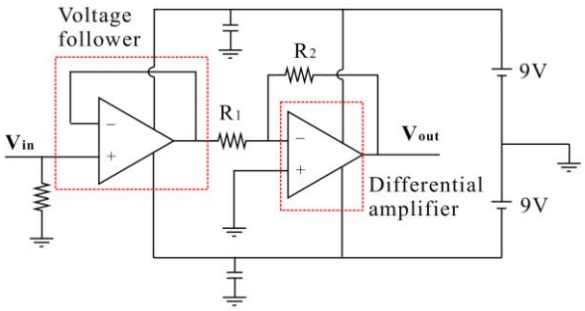


Fig.7 Scheme of the amplifier circuit.

### C. *Signal Capturing Unit*

The signal capturing unit is composed of an amplifier circuit, an A/D converter, and a laptop. The output electric signal of transducer is proportional to the surface displacement on the contact point. At the first stage, this signal is sent to an adjustable amplifier circuit for enhancing the S/N ratio. The output current of the PZT is so small that a voltage follower is adopted as the input buffer of this circuit. At the second stage, a differential voltage amplifier which has high capability of rejecting environmental random noise amplifies the input signal. The scheme of circuit is shown in Fig.7. The gain of the amplifier can be adjusted by changing the resistance ratio of $R_1$ and $R_2$. The output signal $V_{out}$ can be calculated from the formula below:

$$V_{out} = -\frac{R_2}{R_1} V_{in} \qquad (4)$$

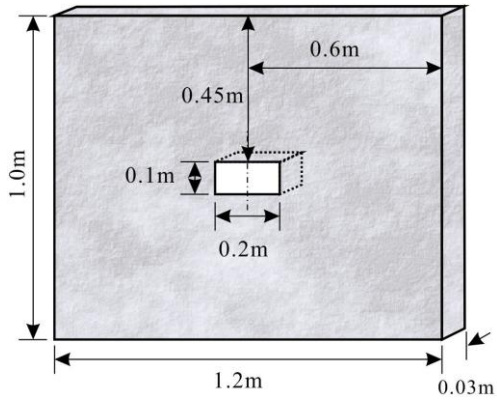


Fig.8 Scheme of concrete specimen with a rectangular void.

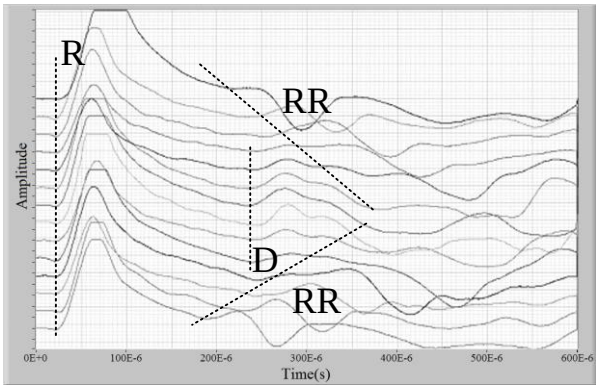


Fig.9 B-scan diagram of concrete specimen with single rectangular void.

Where $V_{in}$ is the input signal. The amplified analog signal is digitized by a PCMCIA interfaced A/D converter for further process. The sampling rate of that converter is 20MSPS which is high enough for the elastic wave signal measurement on civil NDT application. Typically the frequency of elastic wave used in these methods is around 1kHz to 100kHz. The laptop can control the signal capturing procedure and process the captured signals further to form the resultant images.

### *D. Operation Software*

Operation software is essential for a PC-based instrument. It drives the hardware and then processes data when applying the scanning system to in-situ applications. By operating the virtual panel in the software, operator can configure the hardware, input the parameters of measurement and finally get the image. For getting higher resolution signals in amplitude axis, the A/D card should be properly tuned according to the received signals. Besides, the determination of time origin on each received signal is a very important parameter for constructing an image in SAFT-imaging method. In this system, the software will find the arrival time of Rayleigh wave automatically and then define the time origin of each received signal. To prevent the variant impact force of each measurement on affecting the SAFT process, the received signals will be normalized basing on the amplitude of Rayleigh wave. The normalized B-scan traces will then be processed into a gray-leveled SAFT image.

## IV. Experimental Results

To evaluate the feasibility of the new NDT system proposed in this paper, some defective concrete slabs were cased for experiment. The experiment was then carried out with a series of impact-and-receive operations on the top surface of concrete slab. The elastic wave was generated by impacting the specimen's surface with the free fall of an 8 mm steel ball. Distance between the impacting source and the receiver is always set to be 5cm. Measurement gap is kept 5cm. The first measurement was performed at the point which is 30cm from the edge of concrete slab. For each specimen, 14 displacement traces were recorded for further process. To accomplish the artificial void, a styrofoam bar with a wood cover was instead fixed at the design position when the concrete was cast to form the specimen. After curing and removing the form, the styrofoam bar and its wood cover were removed.

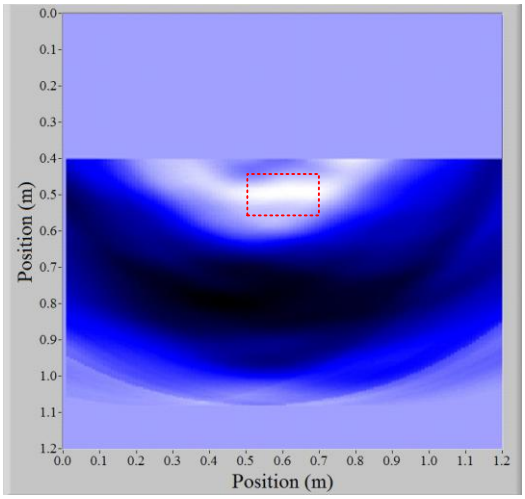


Fig.10 SAFT image generated from displacement responses of concrete specimen with single defect.

### *A. Single Defect Specimen*

Shown in Fig.8 is the scheme of the concrete specimen with an artificial defect inside. The B-scan diagram shown in Fig.9 is composed of 14 displacement traces recorded from a series of impact-and-receive operations on this specimen's surface. In the B-scan diagram, it is not hard to find the P-wave which is reflected from the upper surface of the defect, as marked with "D" in the diagram. Fig.10 is the SAFT image processed with these traces. The image reveals the defect with a bright zone at the center which coincides with the position of the artificial defect inside the concrete specimen. The dotted rectangle in the image represents the location of real defect. In Fig.10, the defect's border doesn't seem very clear. To enhance the contrast of the image, the displacement traces were differentiated numerically into velocity traces. Shown in Fig.11 is the new SAFT image generated from these velocity traces. It is quite obvious that the location, size and front-end shape of the defect are much easier to identify from this image. The experimental result shows good agreement with numerical simulation shown before.

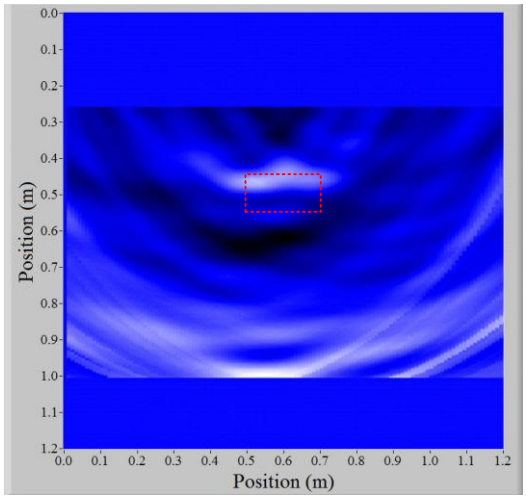


Fig.11 SAFT image generated from velocity responses of concrete specimen with single defect.

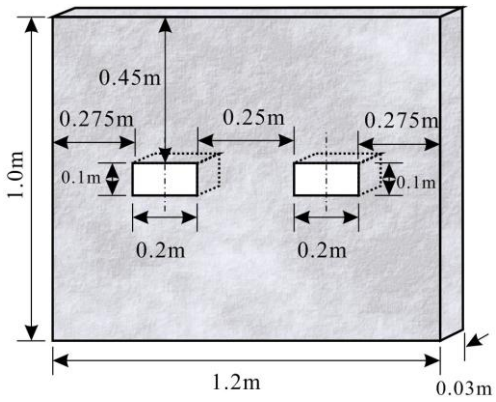


Fig.12 Dimensions of concrete specimen with double defects.

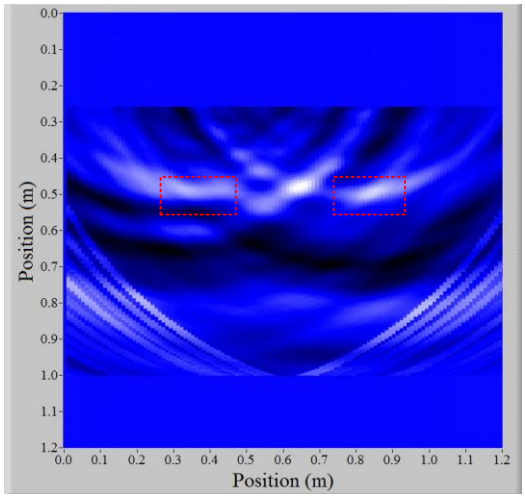


Fig.13 SAFT image generated from velocity responses of concrete specimen with double defects.

### *B. Double Defects Specimen*

In order to test this system's capability of revealing multiple defects inside real concrete, a specimen with two rectangular voids was cast for experiment as shown in Fig.12. The SAFT image of this specimen generated from 14 velocity traces is shown in Fig.13. In this image, the exact positions of defect are marked with two dotted rectangles. At each rectangle, there is a bright strip representing the defect's upper surface. There is one thing to note that there is a bright spot in the middle of two defects. It might come from the reflected Rayleigh wave in the trace which is received at the point near the edge of specimen. Fortunately, boundaries are not always so close to the measurement point when applying this method to in-situ structures.

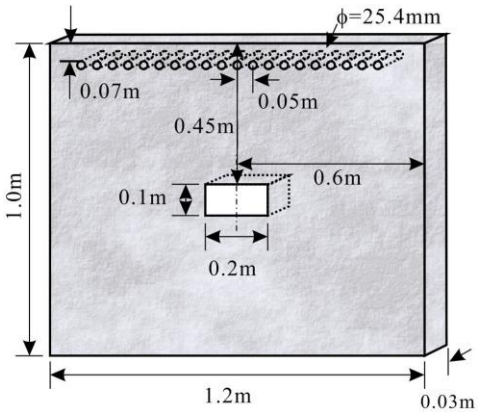


Fig.14 Dimensions of concrete specimen with single rectangular void and single layer rebar.

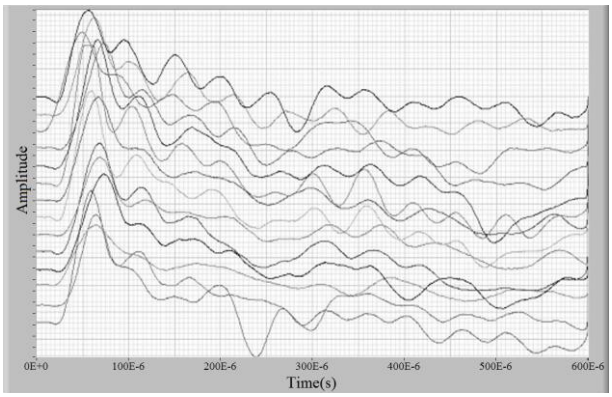


Fig.15 B-scan displacement diagram of concrete specimen with single defect and single layer rebar.

### *C. Single Defect Specimen with Single Layer Rebar*

For most concrete structures, rebar is always indispensable to help structure to resist tension. In order to know if the existence of rebar will affect the exposure of image, a concrete specimen with single layer rebar was cast as shown in Fig.14. The depth of concrete cover is 7cm and the space between two rebar is kept 5cm. In the slab, a rectangular void is beneath the rebar layer. Shown in Fig.15 is the B-scan displacement diagram with 14 received traces. The scattering from rebar affects the received signal severely so that the reflection from defect is hard to define in these time-domain traces. Shown in Fig.16 is the SAFT image generated from these traces. In this image, a bright strip representing the defect's surface can be easily found at the center, even though there are some fuzzy spots induced by scattering of rebar. This case demonstrates that this new NDT system has the capability of exposing the void inside concrete

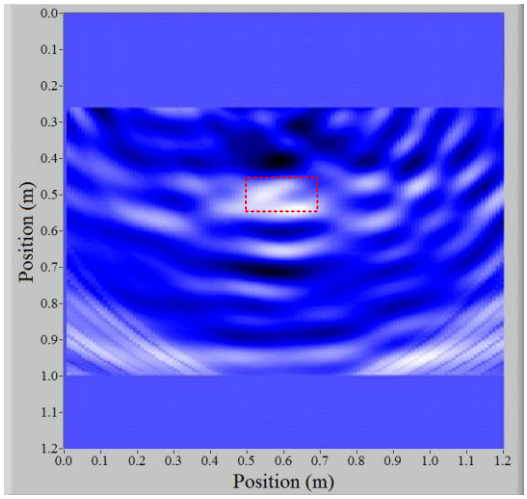


Fig.16 SAFT image generated from velocity responses of concrete specimen with single rectangular void and single layer rebar.

structures despite there is a rebar layer near the inspecting surface.

## V. Conclusion

A well developed instrument is indispensible for a new NDT method when it is applied to inspect the in-situ concrete structures. The state-of-the-art technologies could provide enough assistance to develop the instrument on reducing the size and simplifying the operation procedure. In this paper, a brand new NDT system for defects imaging was proposed. It integrates the point-source/point-receiver scheme with SAFT process. The resultant image can expose the defects embedded inside the concrete structures immediately after a series of impact-and-receive operations. With the aid of this system, the experimental result obtained from the single defect specimen shows good agreement with the numerical result not only on the B-scan diagram but also on the SAFT image. Besides, it can make the resultant image clearer with the numerical differentiation process. To evaluate the feasibility of this NDT system, three concrete slabs with different configuration were cast for experiment. The experimental result shows this system's capability of exposing the defects in real concrete slab by image which can provide the information including location, size and even front-end shape of the defects. There is one more thing need to note that it can reveal the defect despite there is a rebar layer near the concrete's surface. It shows great potential of this new NDT system on detecting defects embedded inside the in-situ concrete infrastructures.

## References

[1] Wu, T. T., Fang, J. S., and Liu, P. L., J. Acoust. Soc. Am., 97, 1678-1686 (1995).
[2] Wu, T. T., Fang, J. S., Liu, G. Y. and Kuo, M. K., J. Acoust. Soc. Am., 98, n4, 2142-2148 (1995).
[3] Carino, N. J., Sansalone, M. and Hsu, N., ACI J., Proceeding, 83, 199-208 (1986).
[4] Oral Büyüköztürk, NDT E Int., 31, n4, 233-243 (1998).
[5] J.-H. Tong, T.-T. Wu and C.-K. Lee, Jpn. J. Appl. Phys., 41, p1, n11A, 6595-6600(2002).
[6] Shu-Tao Liao , Jian-Hua Tong , Cheng-Hou Chen , and Tsung-Tsong Wu, Int. J. Solids Struct., 43/ 7-8, 2279-2298 (2006).
[7] Doctor, S. R., Hall, T. E. and Ried, L. D., NDT E Int., 19, 163-167 (1986).
[8] Waszak, J. and Ludwig, R., "Three-Dimensional Ultrasonic Imaging Employing a Time-Domain Synthetic Aperture Focusing Technique," IEEE Trans. Instrum. Meas., 39, n2, 441-444 (1990).
[9] Jian-Hua Tong, Shu-Tao Liao, Chao-Ching Lin (2007), IEEE Trans. Ultrason. Ferroelectr. Freq. Control , 54, n1, 128-137 (2007).